Cell Death and Differentiation (2015) 22, 2046–2057

www.nature.com/cdd

Regulators of G protein signaling 12 promotes osteoclastogenesis in bone remodeling and pathological bone loss

X Yuan[1], J Cao[2], T Liu[1], Y-P Li[3], F Scannapieco[1,4], X He[5], MJ Oursler[6], X Zhang[7], J Vacher[8], C Li[1], D Olson[1] and S Yang*[,1,4]

Regulators of G protein signaling (Rgs) have pivotal roles in controlling various cellular processes, such as cell differentiation. How Rgs proteins regulate osteoclast (OC) differentiation, function and bone homeostasis is poorly understood. It was previously demonstrated that Rgs12, the largest protein in the Rgs family, is predominantly expressed in OCs and regulates OC differentiation *in vitro*. To further understand the role and mechanism of Rgs12 in OC differentiation and bone diseases *in vivo*, we created OC-targeted *Rgs12* knockout mice by using inducible Mx1-Cre and CD11b-Cre. Deletion of *Rgs12* in hematopoietic cells or specifically in OC precursors resulted in increased bone mass with decreased OC numbers. Loss of *Rgs12* impaired OC differentiation and function with impaired Ca^{2+} oscillations and reduced nuclear factor of activated T cells (NFAT) 2 expression. The introduction of wild-type osteoblasts did not rescue the defective osteoclastogenesis. Ectopic expression of NFAT2 rescued defective OC differentiation in CD11b;$Rgs12^{fl/fl}$ cells and promoted normal OC differentiation. Moreover, deletion of *Rgs12* significantly inhibited pathological osteoclastogenesis and bone destruction in *Rgs12*-deficient mice that were subjected to ovariectomy and lipodysaccharide for bone loss. Thus our findings demonstrate that Rgs12 is an important regulator in OC differentiation and function and identify Rgs12 as a potential therapeutic target for osteoporosis and inflammation-induced bone loss.
Cell Death and Differentiation (2015) **22,** 2046–2057; doi:10.1038/cdd.2015.45; published online 24 April 2015

Bone homeostasis is tightly regulated by the balance between osteoblasts (OBs), the bone-forming cells, and osteoclasts (OCs), the bone-resorbing cells.[1] Pathological conditions such as osteoporosis, inflammation, and cancer break this balance in favor of the augmentation of OC activity, resulting in net bone loss.[2–4] As a result, patients with these diseases suffer from pain and risk of bone fracture. Therefore, understanding OC differentiation and function and uncovering potential therapeutic targets are very important and urgent objectives for treatment of these diseases.[5,6]

Mature OCs, derived from the monocyte/macrophage hematopoietic lineage, are multinucleated and tartrate-resistant acid phosphatase (TRAP) positive.[7] The breakthrough in understanding osteoclastogenesis came from the discovery that receptor activator of NF-κB ligand (RANKL) and macrophage colony-stimulating factor (M-CSF) have essential roles in stimulating monocyte-macrophage lineage cells to differentiate into mature and functional OCs.[8–10] Currently, known crucial RANKL downstream transcription factors and genes include active nuclear factor of activated T cells (NFAT) 2, c-Fos, β_3-integrin, Cathepsin K, and matrix metallopeptidase 9.[11,12] Among these, NFAT2 acts as a master switch for the terminal differentiation of OCs.[13] Robust induction of NFAT2 is dependent on calcium (Ca^{2+}) oscillations.[14] Ca^{2+} oscillations lead to calcineurin-mediated activation of NFAT2 and ensure NFAT2 long-lasting transcriptional activation.[13,14] Despite these new insights, it remains unclear which factor(s) induced by RANKL initiate and maintain Ca^{2+} oscillations and how Ca^{2+} oscillations regulate OC differentiation.

Rgs12 is the largest protein in the Rgs (regulators of G-protein signaling) family.[15] Rgs12 has a PDZ (PSD-95/Dlg/ZO-1) domain, a phosphotyrosine-binding domain, a conserved RGS domain, tandem Ras-binding domains, and a GoLoco interaction motif.[15–17] Its multi-domain structure allows Rgs12 to function as a signaling transduction nexus to modulate multiple signaling pathways.[17–20] It was previously shown that, *in vitro*, Rgs12 expression gradually increases during OC differentiation and that silencing Rgs12

[1]Department of Oral Biology, University at Buffalo, School of Dental Medicine, The State University of New York, Buffalo, NY 14214, USA; [2]USDA Grand Forks Human Nutrition Research Center, Grand Forks, ND 58202, USA; [3]Department of Pathology, University of Alabama at Birmingham (UAB), Birmingham, AL 35294, USA; [4]Developmental Genomics Group, New York State Center of Excellence in Bioinformatics and Life Sciences, University at Buffalo, The State University of New York, Buffalo, NY 14203, USA; [5]Department of Stomatology, The Fourth Affiliated Hospital of China Medical University, China Medical University, Shenyang, Liaoning 110032, China; [6]Department of Medicine, Endocrine Research Unit, Mayo Clinic, Rochester, MN 55905, USA; [7]Department of Orthopedics, Center for Musculoskeletal Research, University of Rochester Medical Center, School of Medicine and Dentistry, Rochester, NY 14642, USA and [8]Department of Medicine, Division of Experimental Medicine, The Institut de Recherches Cliniques de Montréal, University of Montreal, Montreal, Quebec H2W 1R7, Canada

*Corresponding author: S Yang, Department of Oral Biology, University at Buffalo, School of Dental Medicine, The State University of New York, Buffalo, NY 14214, USA. Tel: +1 716 829 6338; Fax: +1 716 829 3942; E-mail: sy47@buffalo.edu

Abbreviations: Ca^{2+}, Calcium; Rgs, regulators of G-protein signaling; OC, osteoclast; OB, osteoblast; TRAP, tartrate-resistant acid phosphatase; M-CSF, macrophage colony-stimulating factor; poly I:C, polyinosinic-polycytidylic acid; LPS, lipodysaccharide; OVX, ovariectomy; BV/TV, bone volume to total bone volume; Tb.Th, trabecular thickness; Tb.N, trabecular number; MNC, multinucleated OC; BFR/BS, bone formation rate; MAR, mineral apposition rate; IL, interleukin; TLR2, Toll-like receptors 2; RANKL, receptor activator of NF-κB ligand; NFAT, nuclear factor of activated T cells; MSC, mesenchymal stem cell

Received 31.12.14; revised 03.3.15; accepted 10.3.15; Edited by M Piacentini; published online 24.4.15

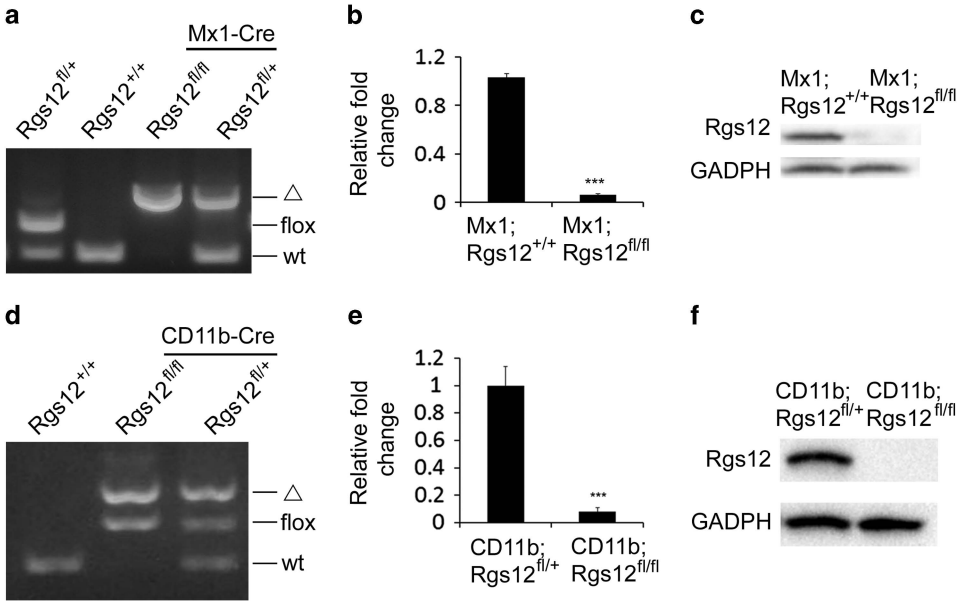

Figure 1 Deletion of Rgs12 in hematopoietic cells (Mx1;Rgs12$^{fl/fl}$) and OCs (CD11b;Rgs12$^{fl/fl}$) reduces Rgs12 expression. (**a** and **d**) PCR of spleen genomic DNA showed the deletion allele of *Rgs12* in Mx1;Rgs12$^{fl/fl}$ and CD11b;Rgs12$^{fl/fl}$ mice. (**b** and **e**) qPCR results showed less *Rgs12* mRNA expression in the spleen of Mx1;Rgs12$^{fl/fl}$ and CD11b-positive bone marrow cells of CD11b;Rgs12$^{fl/fl}$. The expression of Rgs12 was normalized to GAPDH (glyceraldehyde 3-phosphate dehydrogenase) expression ($n=3$, $^{***}P<0.001$ *versus* controls). (**c** and **f**) Western blotting analysis of Rgs12 expression in the bone marrow cells of Mx1;Rgs12$^{fl/fl}$ and CD11b-positive bone marrow cells of CD11b;Rgs12$^{fl/fl}$

blocks OC differentiation, which suggests that Rgs12 is an important regulator of OC differentiation.[21] However, how Rgs12 regulates Ca^{2+} oscillations and OC differentiation during bone development and remodeling *in vivo* is unknown. For this study, we created two strains of OC-targeted *Rgs12* knockout mice – CD11b;Rgs12$^{fl/fl}$ and Mx1;Rgs12$^{fl/fl}$ mice. This was done by crossing Rgs12$^{fl/fl}$ mice with either CD11b-Cre or Mx1-Cre transgenic mice, respectively. CD11b-Cre mice express Cre recombinase during myeloid differentiation under the control of the CD11b promoter. This strain is a useful tool for the study of gene function during OC and macrophage differentiation from embryonic stage.[22] Mx1-Cre mice express Cre recombinase in hematopoietic lineage cells, including early stage OC progenitor cells, and is induced by polyinosinic-polycytidylic acid (poly I:C).[23,24] This strain makes it possible to study gene function at various postnatal bone development and remodeling stages.

We first studied the function of Rgs12 in hematopoietic cells, specifically in OC precursors, *in vivo*. We further analyzed how loss of Rgs12 affects the RANKL-Ca^{2+} oscillations–NFAT2 signaling pathway. In addition to the physiological condition, we analyzed the role of Rgs12 in various pathological conditions to validate Rgs12 as a potential therapeutic target. We treated CD11b;Rgs12$^{fl/fl}$ mice with lipodysaccharide (LPS) in the calvarial bone in order to mimic inflammation-induced osteoclastogenesis and bone destruction. We also studied the function of Rgs12 in estrogen deficiency-induced osteoporosis using an ovariectomy (OVX) model. Our results demonstrated that Rgs12 is an important regulator in OC differentiation and function and that Rgs12 is a potential therapeutic target for osteoporosis and inflammation-induced bone loss.

Results

Generation of Rgs12 conditional knockout mice. To assess the role of Rgs12 in OC differentiation and function *in vivo*, we crossed Rgs12$^{fl/fl}$ mice[25] with either CD11b-Cre[22] or Mx1-Cre[23] transgenic lines to generate *Rgs12* conditional knockout mice (CD11b;Rgs12$^{fl/fl}$ and Mx1;Rgs12$^{fl/fl}$, respectively). In Mx1;Rgs12$^{fl/fl}$ mice, *Rgs12* was deleted in hematopoietic cells, including OCs, by injecting poly I:C at postnatal days 10, 12, and 14. In CD11b;Rgs12$^{fl/fl}$ mice, *Rgs12* was deleted in the monocyte-OC lineage at embryonic day E10.5. Both CD11b;Rgs12$^{fl/fl}$ and Mx1;Rgs12$^{fl/fl}$ mice were born with the expected Mendelian ratios. Deletion of *Rgs12* was examined using spleen genomic DNA (Figures 1a and d). Low levels of *Rgs12* mRNA in the spleen (Figure 1b) and significantly diminished Rgs12 protein levels in the bone marrow (Figure 1c) were found in Mx1;Rgs12$^{fl/fl}$ mice. CD11b-Cre deletion resulted in partial *Rgs12* deletion in the spleen DNA (Figure 1d), as expected. However, markedly lower *Rgs12* mRNA and protein levels were found in the CD11b-positive cells derived from the bone marrow cells of CD11b;Rgs12$^{fl/fl}$ mice (Figures 1e and f).

Targeted deletion of Rgs12 in hematopoietic cells and OCs in postnatal stage increased cancellous bone mass with decreased OC number. To determine whether deletion of *Rgs12* affects bone physiology, the femurs of 3-month-old Mx1;Rgs12$^{fl/fl}$ mice and their control littermates (Mx1;Rgs12$^{+/+}$) were examined by Micro-CT analysis. Mx1;Rgs12$^{fl/fl}$ mice exhibited a marked increase in cancellous bone mass (Figure 2a). The percentage of bone volume to total bone volume (BV/TV), trabecular number (Tb.N), and trabecular

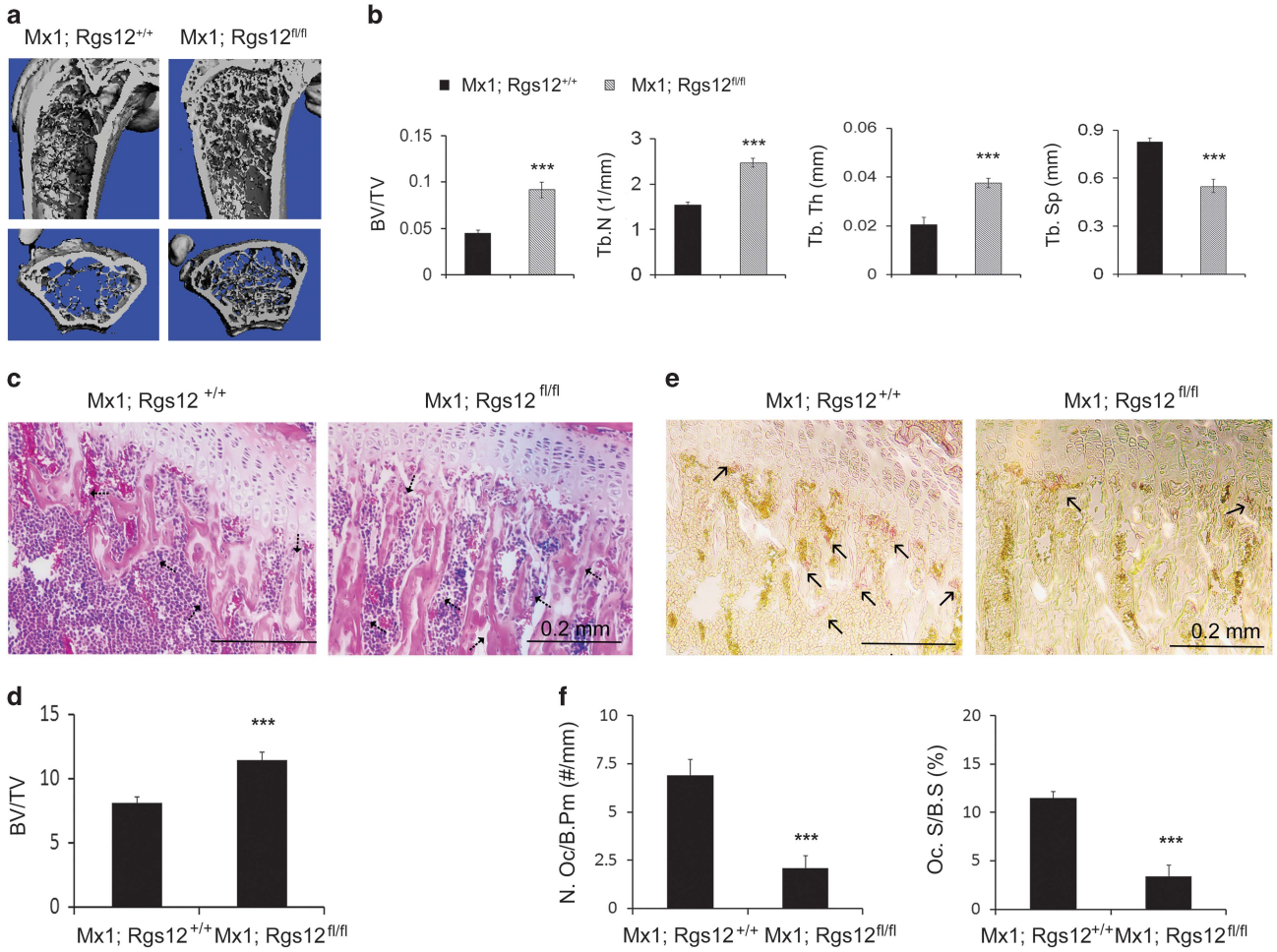

Figure 2 Deletion of *Rgs12* in hematopoietic cells (Mx1;Rgs12$^{fl/fl}$) causes a significant increase in bone mass with reduced OC formation. (**a**) μCT analysis of the femurs of 3-month-old Mx1;Rgs12$^{fl/fl}$ and Mx1;Rgs12$^{+/+}$ (upper photograph: longitudinal view; lower photograph: axial view of the metaphyseal region). An apparent increase in the bone mass was observed in Mx1;Rgs12$^{fl/fl}$ mice compared with Mx1;Rgs12$^{+/+}$ mice. (**b**) Quantitative analysis of bone volume/tissue volume (BV/TV, %), trabecular thickness (Tb.Th, μm), trabecular number (Tb.N, /mm) and trabecular separation (Tb.Sp, μm) in the tibia of Mx1;Rgs12$^{fl/fl}$ and Mx1;Rgs12$^{+/+}$ mice shown in panel (**a**). Results are mean $\pm$ S.D. ($n=4$, ***$P<0.001$). (**c**) Hematoxylin and eosin staining of the proximal tibia metaphyseal regions of 3-month-old Mx1;Rgs12$^{fl/fl}$ and Mx1;Rgs12$^{+/+}$ mice. (**d**) Quantitative analysis of the percentage of bone area to total bone marrow space shown in panel (**c**) ($n=4$, $P<0.001$). (**e**) TRAP staining of tibiae sections shown in panel (**c**) to identify OCs. (**f**) Histomorphometric analysis of osteoclasts in Mx1;Rgs12$^{fl/fl}$ and Mx1;Rgs12$^{+/+}$ mice at 3 months of age ($n=4$, $P<0.001$). N.Oc/B.Pm: number of OCs/bone perimeter (mm); Oc.S/B.S: OC surface/bone surface (%)

thickness (Tb.Th) in the femurs of Mx1;Rgs12$^{fl/fl}$ mice were 2, 1.6, and 1.9-fold of those in control mice, respectively, while trabecular spacing (Tb.Sp) in the femurs of Mx1;Rgs12$^{fl/fl}$ mice was 0.6-fold of that in control mice (Figure 2b, $P<0.001$). To further evaluate bone morphology, histological H&E staining analysis of the tibias from Mx1;Rgs12$^{fl/fl}$ and Mx1;Rgs12$^{+/+}$ mice was performed (Figure 2c). Compared with the control mouse tibia, Mx1;Rgs12$^{fl/fl}$ mouse tibia exhibited a significant increase in the trabecular bone and cortical bone. Quantitative analysis confirmed that bone area in Mx1;Rgs12$^{fl/fl}$ mice was 1.5-fold of that in controls (Figure 2d, $P<0.001$). To visualize OCs, the tibia histological sections were stained for TRAP activity. The OC number in Mx1;Rgs12$^{fl/fl}$ tibia was 0.28-fold of that in control mice (Figures 2e and f, $P<0.001$). Moreover, the TRAP^{+} area in Mx1;Rgs12$^{fl/fl}$ mice was about 0.33-fold of that in control mice (Figures 2e and f, $P<0.001$). This data demonstrated that the postnatal deletion of *Rgs12* in early-stage OC progenitor cells impaired OC differentiation and caused osteopetrosis phenotype.

Targeted deletion of Rgs12 in hematopoietic cells and OCs of embryonic stage increased bone mass. To investigate Rgs12 functions in OC differentiation in the embryonic stage, we further analyzed CD11b;Rgs12$^{fl/fl}$ mice. As we found that there is no difference in both bone phenotype and *in vitro* experiments between CD11b;Rgs12$^{fl/fl}$ and CD11b;Rgs12$^{fl/+}$ (data not shown), we chose CD11b;Rgs12$^{fl/+}$ as a control due to breeding convenience. Similar to Mx1;Rgs12$^{fl/fl}$ mice, CD11b;Rgs12$^{fl/fl}$ mice had significantly greater bone mass in the femurs at 3 months of age ($P<0.001$), as determined by comparing the cancellous bone volumes (Figure 3a). However, CD11b;Rgs12$^{fl/fl}$ mice had a milder skeletal phenotype than Mx1;Rgs12$^{fl/fl}$ mice. The BV/TV, Tb.N, and Tb.Th in the femurs of CD11b;Rgs12$^{fl/fl}$ mice were 1.4, 1.3, and 1.1-fold of those in CD11b;Rgs12$^{fl/+}$

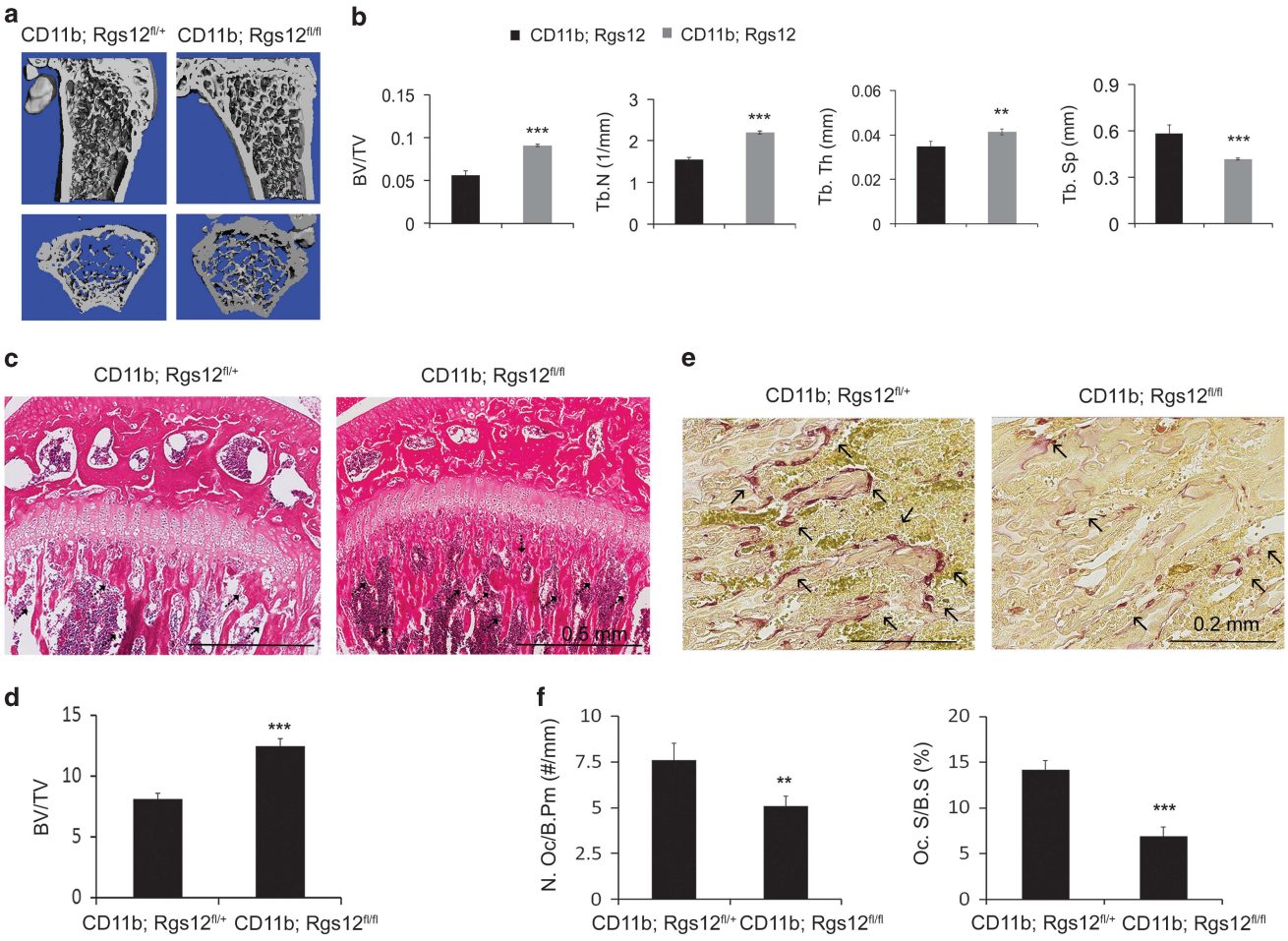

Figure 3 Deletion of *Rgs12* in OCs (CD11b;Rgs12fl/fl) causes a significant increase in bone mass. (**a**) μCT analysis of the femurs of 3-month-old CD11b;Rgs12$^{fl/fl}$ and CD11b;Rgs12$^{fl/+}$. (**b**) Quantitative analysis of BV/TV (%), Tb.Th (μm), Tb.N (/mm), and Tb.Sp (μm) in the tibia of CD11b;Rgs12$^{fl/fl}$ and CD11b;Rgs12$^{fl/+}$ mice shown in panel (**a**). Results are mean $\pm$ S.D. ($n=4$, $^{**}P<0.01$, $^{***}P<0.001$). (**c**) Hematoxylin and eosin staining of the proximal tibia metaphyseal regions of CD11b;Rgs12$^{fl/fl}$ and CD11b;Rgs12$^{fl/+}$ mice at 3 months. (**d**) Quantitative analysis of the percentage of bone area to total bone marrow space shown in panel (**c**) ($n=4$, $P<0.001$). (**e**) TRAP staining of tibiae sections shown in panel (**c**) to identify OCs. (**f**) Histomorphometric analysis of OCs in CD11b;Rgs12$^{fl/fl}$ and CD11b;Rgs12$^{fl/+}$ mice at 3 months of age. $n=4$, $^{**}P<0.01$, $^{***}P<0.001$

mice, respectively (Figure 3b). Histomorphometric analysis confirmed the bone mass increase in CD11b;Rgs12$^{fl/fl}$ mice (Figures 3c and d). Moreover, the OC number and TRAP$^+$ area in the CD11b;Rgs12$^{fl/fl}$ tibia was 0.66- and 0.48-fold of that in the tibia of CD11b;Rgs12$^{fl/+}$ mice, respectively (Figures 3e and f). As CD11b-Cre deleted *Rgs12* in the embryonic stage, we stained the newborn CD11b;Rgs12$^{fl/+}$ and CD11b;Rgs12$^{fl/fl}$ mice with Alizarin Red and Alizarin Blue to visualize the whole skeleton (Supplementary Figure S1). The results showed that there were not significant differences in bone formation between newborn CD11b;Rgs12$^{fl/+}$ and newborn CD11b;Rgs12$^{fl/fl}$ mice, which suggests that Rgs12 does not significantly affect bone development in the embryonic stage.

Deletion of Rgs12 impaired OC differentiation. To further analyze the role of Rgs12 in osteoclastogenesis, OC precursor cells from the bone marrow of 1-month-old CD11b;Rgs12$^{fl/fl}$ and the control mice were induced with RANKL and M-CSF *in vitro*. TRAP staining results revealed that most of bone marrow cells from the control mice differentiated into TRAP$^+$ multinucleated OCs (MNCs) (Figure 4a); however, only a few TRAP$^+$ MNCs were found in the CD11b;Rgs12$^{fl/fl}$ group. The number of TRAP$^+$ MNCs from CD11b;Rgs12$^{fl/fl}$ mice were only 0.25-fold of that from control mice (Figure 4b, $P<0.001$). Furthermore, the MNCs size and the number of nuclei per MNC significantly decreased in the CD11b;Rgs12$^{fl/fl}$ group (Figure 4b).

OCs can be generated *in vitro* from bone marrow–derived OC precursors when co-cultured with OB cells in the presence of 1α, 25-dihydroxyvitamin D_3 and dexamethasone.[26] These activated OBs can provide M-CSF and RANKL to support OC formation.[27] Thus we investigated whether co-culture of CD11b;Rgs12$^{fl/fl}$ bone marrow cells with wild-type primary OBs was able to rescue the defective osteoclastogenesis. Wild-type OBs were found to support OC precursor cells derived from CD11b;Rgs12$^{fl/+}$ for the generation of giant TRAP$^+$ MNCs (Figure 4c). However, the OB cells failed to support the differentiation of CD11b;Rgs12$^{fl/fl}$ bone marrow cells (Figures 4c and d, $P<0.001$). Our results demonstrated

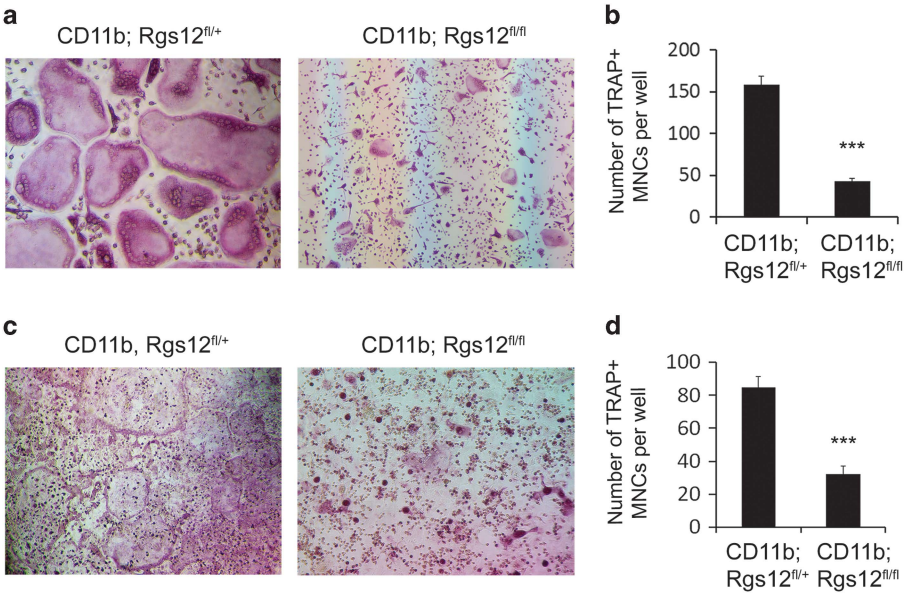

Figure 4 Rgs12 is essential for OC differentiation. (**a**) TRAP staining of control and CD11b;Rgs12$^{fl/fl}$ OCs derived from bone marrow OC precursor cells in response to RANKL and M-CSF. (**b**) Quantification of the number of TRAP^{+} multinucleated OCs (MNCs) shown in panel (**a**) ($n=4$, $P<0.001$). (**c**) OC differentiation from control and CD11b; Rgs12$^{fl/fl}$ bone marrow cells in coculture with wild-type OBs. (**d**) Quantification of the number of TRAP^{+} MNCs shown in (**c**) ($n=4$, $P<0.001$)

that the introduction of wild-type OBs did not rescue the defective osteoclastogenesis and further support that Rgs12 is crucial for OC differentiation.

Deletion of Rgs12 impaired OC function. As deletion of *Rgs12* causes defective OC differentiation, we further studied the effects of Rgs12 loss on OC function. F-actin ring podosome belt formation is a prerequisite for OC bone resorption.[28,29] We used rhodamine–phalloidin staining to assess F-actin ring formation in primary OCs induced by M-CSF/RANKL from the bone marrow cells of the control and CD11b;Rgs12$^{fl/fl}$ mice. About 60% of OCs from the control mice had complete and organized F-actin rings; whereas, only about 40% of OCs from CD11b;Rgs12$^{fl/fl}$ mice had well-formed F-actin rings (Figures 5a and b, $P<0.01$). Nearly 60% of the OCs from CD11b;Rgs12$^{fl/fl}$ mice had the disrupted actin rings or no rings. Moreover, the size of disrupted actin rings appeared smaller than the size of the actin rings in the control group. We further confirmed these results by using an OB–OC co-culture system (Figures 5c and d, $P<0.01$). This data suggest that Rgs12 has an important role in organizing OC-specific cytoskeleton and regulates OC function and bone resorption. To further investigate OC function, we utilized a dentin bone resorption assay. The OC cultures of CD11b;Rgs12$^{fl/fl}$ resulted in significantly less resorbed areas on the elephant dentin slides than did the control group (Figures 5e and f). This indicates that deletion of *Rgs12* impairs OC-mediated bone resorption. These results confirmed the importance of Rgs12 as a regulator of OC function.

Deletion of Rgs12 inhibited Ca^{2+} oscillations and NFAT2 expression, and ectopic expression of NFAT2 rescued defective OC differentiation in CD11b;Rgs12$^{fl/fl}$ cells. To gain further insight into the mechanism underlying the regulation of Rgs12 in OC differentiation, we investigated the essential transcription factors and marker genes for OC formation and function. Compared with the control cells, Rgs12-deficient OC progenitor cells had significantly lower expression of NFAT2, c-Fos (transcription factors required for OC differentiation) and Cathepsin K (required for bone resorption) at 24 h after RANKL stimulation (Figure 6a). These results further confirmed that osteoclastogenesis was impaired in the CD11b;Rgs12$^{fl/fl}$ group. Accumulating studies showed that Rgs proteins have a critical role in regulating Ca^{2+} oscillations in various cells, including pancreatic acinar cells and T lymphocytes,[30–33] and that Ca^{2+} oscillations and NFAT2 activation are essential for RANKL-induced OC differentiation.[13] Thus we hypothesized that Rgs12 is a specific regulator of Ca^{2+} oscillations in response to RANKL during OC differentiation. To test this hypothesis, we used Fluo4 to monitor the internal Ca^{2+} concentration after CD11b; Rgs12$^{fl/fl}$ and CD11b;Rgs12$^{fl/+}$ mouse bone marrow cells were treated with RANKL and M-CSF for 24 h. Ca^{2+} oscillations occurred at approximately 2-min intervals in the control cells (Figure 6b, left panel), while the RANKL-induced Ca^{2+} oscillations were barely detectable in CD11b;Rgs12$^{fl/+}$ cells (Figure 6b, right panel), which correlated with reduced NFAT2 expression (Figure 6a). Similar results were obtained when testing bone marrow cells from Mx1;Rgs12$^{fl/fl}$ mice (Supplementary Figure S2).

To further understand the role of Rgs12 in the RANKL–Ca^{2+} oscillations–NFAT2 signaling pathway, we ectopically expressed ca-NFAT2 in OC precursor cells using a retrovirus-mediated gene transfer system.[13] Successful NFAT2 overexpression was confirmed by using qPCR after transfection (Figure 6c). Defective OC differentiation resulting from *Rgs12* deletion was partially rescued by retroviral ectopic expression of ca-NFAT2 (Figures 6d and e). Cathepsin K

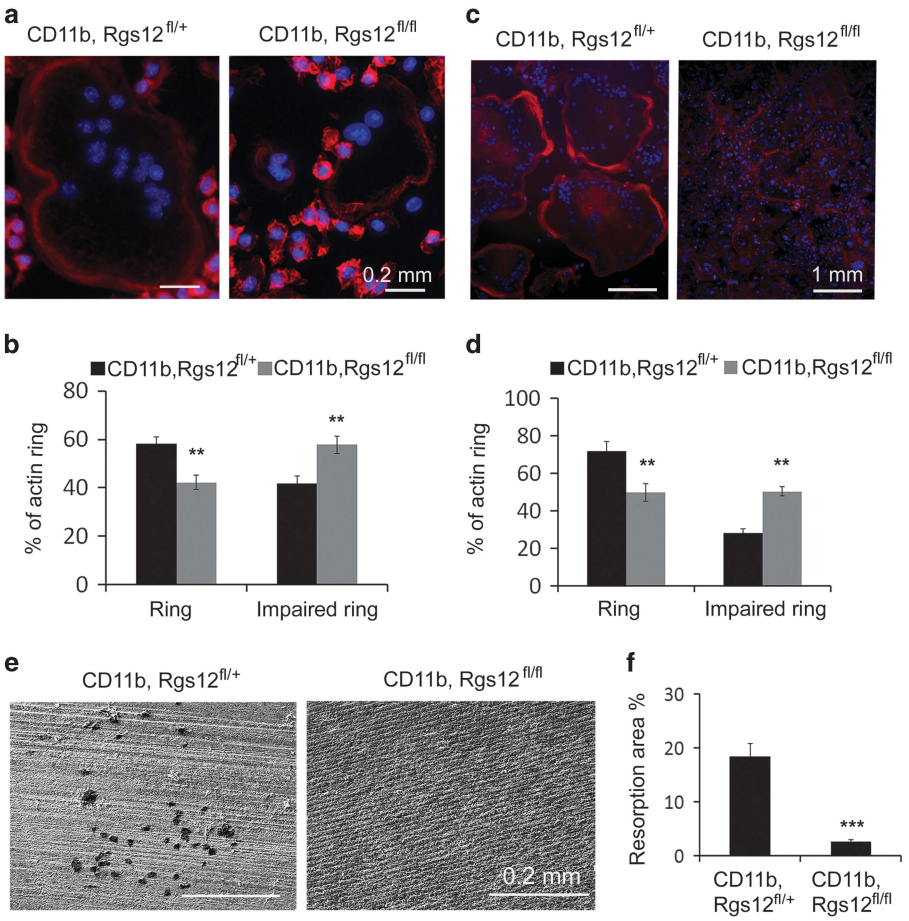

Figure 5 Rgs12 is essential for OC function. (**a**) F-actin ring staining of OCs generated from the bone marrow cells of control and CD11b;Rgs12$^{fl/fl}$ mice. (**b**) Quantification of the number of OCs with intact actin rings or impaired rings illustrated in panel (**a**) ($n=3$, $P<0.01$). (**c**) F-actin ring staining of OCs from control and CD11b;Rgs12$^{fl/fl}$ bone marrow cells in coculture with wild-type OBs. (**d**) Quantification of the number of OCs with actin rings illustrated in panel (**c**) ($n=3$, $P<0.01$). (**e**) Bone resorption lacunae on dentin slices formed by control and Rgs12^{Null} OCs. (**f**) Quantification of the resorption area shown in panel (**e**) ($n=3$, $P<0.001$). $^{**}P<0.01$, $^{***}P<0.001$

expression, but not c-Fos, was significantly upregulated after introducing ca-NFAT2 into *Rgs12*-deficient cells (Figure 6f). These findings support our hypothesis that Rgs12 acts upstream of NFAT2 signaling and has an important role in RANKL–Ca^{2+} oscillations–NFAT2 signaling pathway.

Deletion of Rgs12 in OC precursor cells protected against LPS-induced bone loss. We have shown that Rgs12 has an important role in OC differentiation and bone remodeling under physiological conditions. Next we used a LPS-induced bone resorption model in order to determine whether Rgs12 is involved in inflammation-induced bone loss.[34–37] LPS were injected into the local calvarial region of CD11b;Rgs12$^{fl/fl}$ and CD11b;Rgs12$^{fl/+}$ mice to induce bone destruction. Histological analysis showed that bone erosion was markedly reduced in the CD11b;Rgs12$^{fl/fl}$ group (Figure 7a). Quantitative analysis revealed a greater than two-fold decrease of the osteolytic cavities in CD11b;Rgs12$^{fl/fl}$ group compared with those of the control group (Figure 7b, $P<0.001$). TRAP staining revealed that OC numbers in CD11b;Rgs12$^{fl/fl}$ mice under this pathological condition were significantly lower than those of the control mice (Figures 7c and d, $P<0.001$). These results demonstrated that Rgs12 mediates inflammation-induced osteolysis and that loss of Rgs12 protects against LPS-induced bone loss *in vivo*.

To further determine the role of Rgs12 in LPS-mediated osteoclastogenesis, control and Rgs12-deficient OC precursor cells were cultured *in vitro* and treated with LPS in the presence of M-CSF. TRAP staining revealed that LPS-induced OC differentiation occurred without sustained RANKL stimulation, and deletion of Rgs12 dramatically inhibited LPS-induced OC formation (Figure 7e). The number of TRAP^{+} MNCs in CD11b;Rgs12$^{fl/fl}$ group was only 0.42-fold of the CD11b;Rgs12$^{fl/+}$ group (Figure 7f, $P<0.001$). These results further confirmed that Rgs12 is a positive modulator in pathogenic osteoclastogenesis.

Deletion of Rgs12 protected mice against OVX-induced bone loss. As deletion of Rgs12 in mice under physiological conditions caused osteopetrosis, we next evaluated the effect of the loss of Rgs12 on prevention of estrogen deficiency-induced osteoporosis. To investigate the bone metabolism of adult mice and avoid the confounding factor of growth

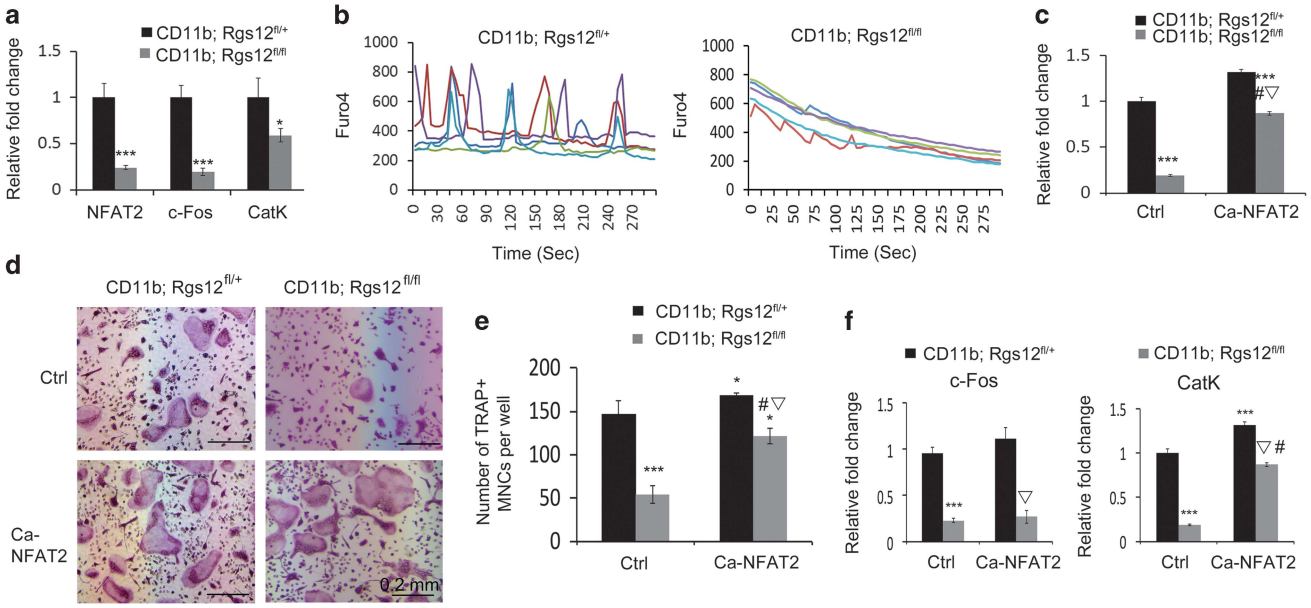

Figure 6 Deletion of *Rgs12* inhibits NFAT2, c-Fos, and Cathepsin K expression and blocks Ca^{2+} oscillations; and ectopic expression of NFAT2 rescues defective OC differentiation. (**a**) qPCR analysis of OC marker gene NFAT2, c-Fos, and Cathepsin K (CatK) expression. GAPDH (glyceraldehyde 3-phosphate dehydrogenase) was used as a loading control, and the expression level of control was set as 1 ($n=3$). (**b**) Analysis of Ca^{2+} oscillations in OCs generated from control and CD11b;$Rgs12^{fl/fl}$ mice at 24 h after RANKL stimulation. Five cells from each group were traced, calculated, and plotted with the time indicated by different colors. (**c**) qPCR analysis of NFAT2 expression in OCs from CD11b;$Rgs12^{fl/+}$ and CD11b;$Rgs12^{fl/fl}$ treated with (Ca-NFAT2) or without (Ctrl) Ca-NFAT2 retrovirus. GAPDH was used as a loading control, and the expression level of control was set as 1 ($n=3$). (**d**) TRAP staining of CD11b;$Rgs12^{fl/+}$ and CD11b;$Rgs12^{fl/fl}$ OCs formed by bone marrow OC precursor cells with or without ca-NFAT2 retrovirus as indicated. (**e**) Quantification of the number of $TRAP^+$ MNCs shown in panel (**d**) ($n=3$). (**f**) qPCR analysis of c-Fos and CatK expression in OC derived from CD11b;$Rgs12^{fl/+}$ and CD11b;$Rgs12^{fl/fl}$ bone marrow OC precursor cells treated with or without Ca-NFAT2 retrovirus. GAPDH was used as a loading control, and the expression level of CD11b;$Rgs12^{fl/+}$ was set as 1 ($n=3$). $^{***}P<0.001$, $^{*}P<0.05$ compared with CD11b;$Rgs12^{+/fl}$; $^{\#}P<0.01$ CD11b;$Rgs12^{fl/fl}$+NFAT2 *versus* CD11b;$Rgs12^{fl/fl}$; $^{\triangledown}P<0.01$ CD11b;$Rgs12^{fl/fl}$+NFAT2 *versus* CD11b;$Rgs12^{fl/+}$+NFAT2

dynamics, OVX was performed on 4-month-old female Mx1;$Rgs12^{fl/fl}$ and Mx1;$Rgs12^{+/+}$ littermates.[38] At 6 weeks after OVX, Mx1;$Rgs12^{fl/fl}$ mice had significantly less bone loss than Mx1;$Rgs12^{+/+}$ controls (Figure 8a). BV/TV, Tb.N, and Tb.Sp in the femurs of Mx1;$Rgs12^{+/+}$ OVX mice were 0.31, 0.3, and 1.84-fold of those in Mx1;$Rgs12^{+/+}$ sham mice (sham operation described in Materials and Methods section), respectively (Figure 8b). However, BV/TV, Tb.N, and Tb.Sp in the femurs of Mx1;$Rgs12^{fl/fl}$ OVX mice were 0.67, 0.56, and 1.83-fold of those in Mx1;$Rgs12^{fl/fl}$ sham mice (Figure 8b). BV/TV of Mx1;$Rgs12^{fl/fl}$ mice was 1.32-fold of that in Mx1;$Rgs12^{+/+}$ mice in the sham groups, but it was 3.33-fold higher in the Mx1;$Rgs12^{fl/fl}$ OVX group than in the Mx1;$Rgs12^{+/+}$ OVX group (Figure 8b). Although Tb.Th slightly decreased in the OVX group for both Mx1;$Rgs12^{+/+}$ and Mx1;$Rgs12^{fl/fl}$, these decreases were not statistically significant (Figure 8b). Histomorphometric analysis revealed that the bone formation rate (BFR/BS, mm^3/mm^2/day) and the mineral apposition rate (MAR; μm/day) in the Mx1;$Rgs12^{+/+}$ and Mx1;$Rgs12^{fl/fl}$ OVXed groups were 0.67- and 0.71-fold of those in the sham groups, respectively (Figure 8c). In sham condition, there is no significant differentiation in MAR and BFR/BS between Mx1;$Rgs12^{+/+}$ and Mx1;$Rgs12^{fl/fl}$ mice. However, deletion of Rgs12 in the absence of estrogen resulted in increased MAR and BFR/BS. MAR in the Mx1;$Rgs12^{fl/fl}$ OVX group was similar to that in the Mx1;$Rgs12^{fl/fl}$ sham group, but the Mx1;$Rgs12^{fl/fl}$ OVX group was about 75% in BFR/BS of that in the Mx1;$Rgs12^{fl/fl}$ sham group (Figure 8c). These findings demonstrated that Rgs12 significantly protected the mice against estrogen deficiency-induced osteoporosis.

Discussion

Rgs proteins are involved in bone remodeling through their influences on OC and OB differentiation and function.[39–42] It was previously demonstrated that Rgs12, the largest protein in the Rgs family, is predominantly expressed in OCs and regulates OC differentiation *in vitro*. To define the role of Rgs12 *in vivo*, we generated *Rgs12* conditional knockout mice.[25] Mx1-Cre targets not only OC precursor cells but also multiple hematopoietic cell types, including megakaryocytes, lymphocytes, mast cells, and monocytemacrophages. To specifically understand the role of Rgs12 in OC lineage *in vivo*, we also generated a specific conditional knockout model with CD11b-Cre for deleting *Rgs12* more exclusively in the OC lineage cells at a relatively early and developmental stage[22] to facilitate understanding of Rgs12 in OC differentiation and function. CD11b;$Rgs12^{fl/fl}$ and Mx1;$Rgs12^{fl/fl}$ mice all displayed skeletal defects such as a marked increase in cancellous bone mass and decreased OC numbers. These observations are consistent with impaired OC differentiation and function of the *Rgs12* mutant. As expected, isolated bone marrow cells exhibited a striking inability to differentiate into OCs. Additionally, although a few $TRAP^+$ OC-like cells were formed in the CD11b;$Rgs12^{fl/fl}$ group, 60% of these cells had impaired cytoskeleton organization and bone resorption.

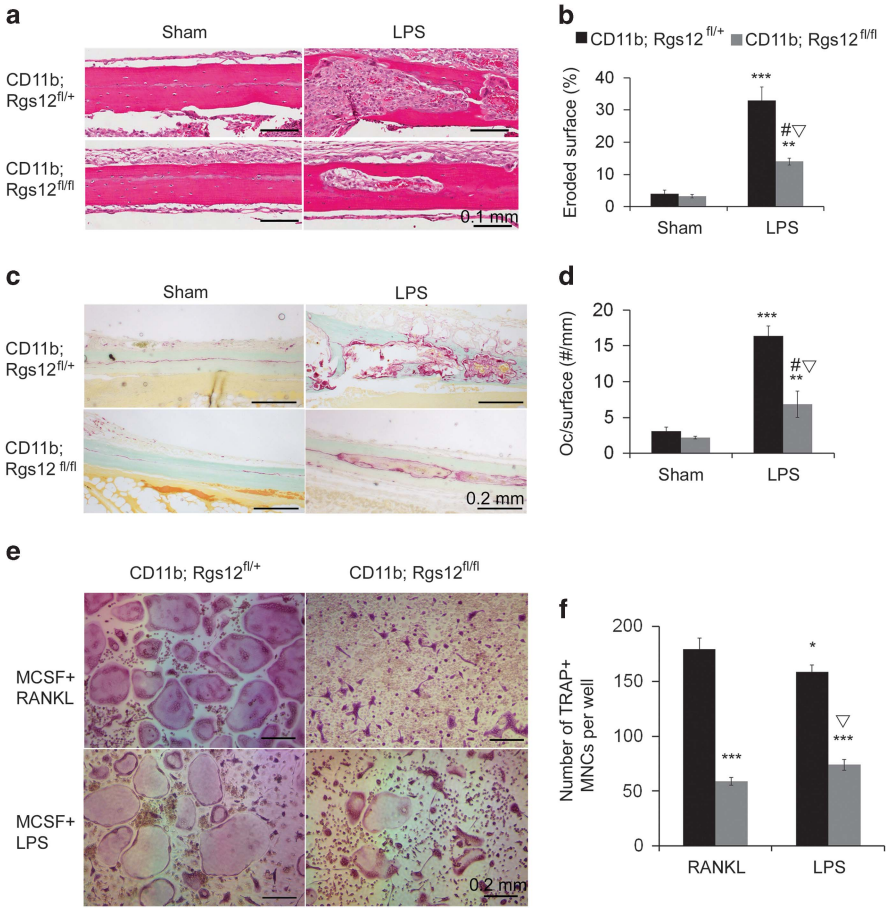

Figure 7 Loss of Rgs12 in OC precursor cells reduced LPS-induced bone loss *in vivo* and OC formation *in vitro*. (**a**) Hematoxylin and eosin staining of calvarial bone injected with PBS (sham) or LPS in CD11b;Rgs12$^{fl/+}$ and CD11b;Rgs12$^{fl/fl}$ mice. (**b**) Quantification of the percentage of eroded surface over total bone surface shown in panel (**a**) ($n=8$). (**c**) TRAP staining of the calvarial bone shown in panel (**a**) to assess OC numbers. (**d**) Quantification of the number of OC per bone surface shown in panel (**c**) ($n=8$). $^{**}P<0.01$, $^{***}P<0.001$ compared with CD11b;Rgs12$^{fl/+}$+sham; $\#P<0.001$ CD11b;Rgs12$^{fl/fl}$+LPS *versus* CD11b;Rgs12$^{fl/fl}$; $\triangledown P<0.001$: CD11b;Rgs12$^{fl/fl}$+LPS *versus* CD11b;Rgs12$^{fl/+}$+LPS. (**e**) TRAP staining of the OC generated by M-CSF/RANKL or M-CSF/LPS as indicated. (**f**) Quantification of the TRAP^{+} MNCs shown in panel (**e**) ($n=3$). $^{***}P<0.001$, $^{*}P<0.05$ compared with CD11b;Rgs12$^{fl/+}$+RNAKL; $\triangledown P<0.001$: CD11b;Rgs12$^{fl/fl}$+LPS *versus* CD11b;Rgs12$^{fl/+}$+LPS

Our results further showed that Rgs12-deficient OC lineage cells lacked Ca^{2+} oscillations in response to RANKL and therefore reduced NFAT2 expression. In addition to RANKL–$[Ca^{2+}]_i$ oscillation–NFATc1 pathway, Rgs12 also regulates c-fos expression; this suggested that Rgs12 may be involved in RANKL–JNK–c-Fos pathway.[43] Overexpression of NFAT2 partially restored the differentiation ability and Cathepsin K expression but not c-Fos expression in Rgs12-deficient OC precursor cells. This is supported by the findings from Takayanagi *et al.* that NFAT2 cooperates with c-Fos to lead to OC differentiation and that overexpression of NFAT2 can only partially restore the osteoclastogenesis in *NFAT2*-mutant cells.[13] Therefore, we can explain that reduced expression of c-fos restricted from the full restoration. Thus, our findings indicate that Rgs12 acts in the downstream of RANKL and upstream of NFAT2 and has a critical role in the regulation of RANKL–Ca^{2+} oscillations–NFAT2 pathway during OC differentiation and function.

In addition to the role that Rgs12 has in physiological conditions, we found that Rgs12 mediates osteoclastogenesis and bone loss after LPS challenge. Previous studies have indicated that LPS causes bone destruction by inducing interleukin-1 (IL-1), IL-11, prostaglandins, and tumor necrosis factor receptor signaling.[34,44] These cytokines may be secreted by OBs, fibroblasts, or immune cells upon LPS stimulation and stimulate OC precursor, accelerating osteoclastogenesis. In both models, we found that deletion of Rgs12 inhibits LPS-induced bone loss, suggesting impaired osteoclastogenesis in the CD11b;Rgs12$^{fl/fl}$ OC precursors protect the mice from cytokine-driven bone loss. In addition to stimulating OBs, fibroblasts, or immune cells, it is also possible that LPS directly triggers Toll-like receptors 2 (TLR2) and TLR4 in pre-OCs or OC precursor cells to promote OC differentiation.[45,46] Liu *et al.*[47] reported that LPS has bi-functional roles in osteoclastogenesis *in vitro*. LPS stimulates NFAT2 expression in RANKL-pretreated cells and therefore promotes osteoclastogenesis. However, LPS abolishes RANKL-induced NFAT2 expression in freshly isolated OC precursors. In our study, the OC precursor cells in bone marrow were pretreated with RANKL for 36 h and then induced with 100 ng/ml LPS for additional 5 days. TRAP staining revealed a significant fewer in OC number in the

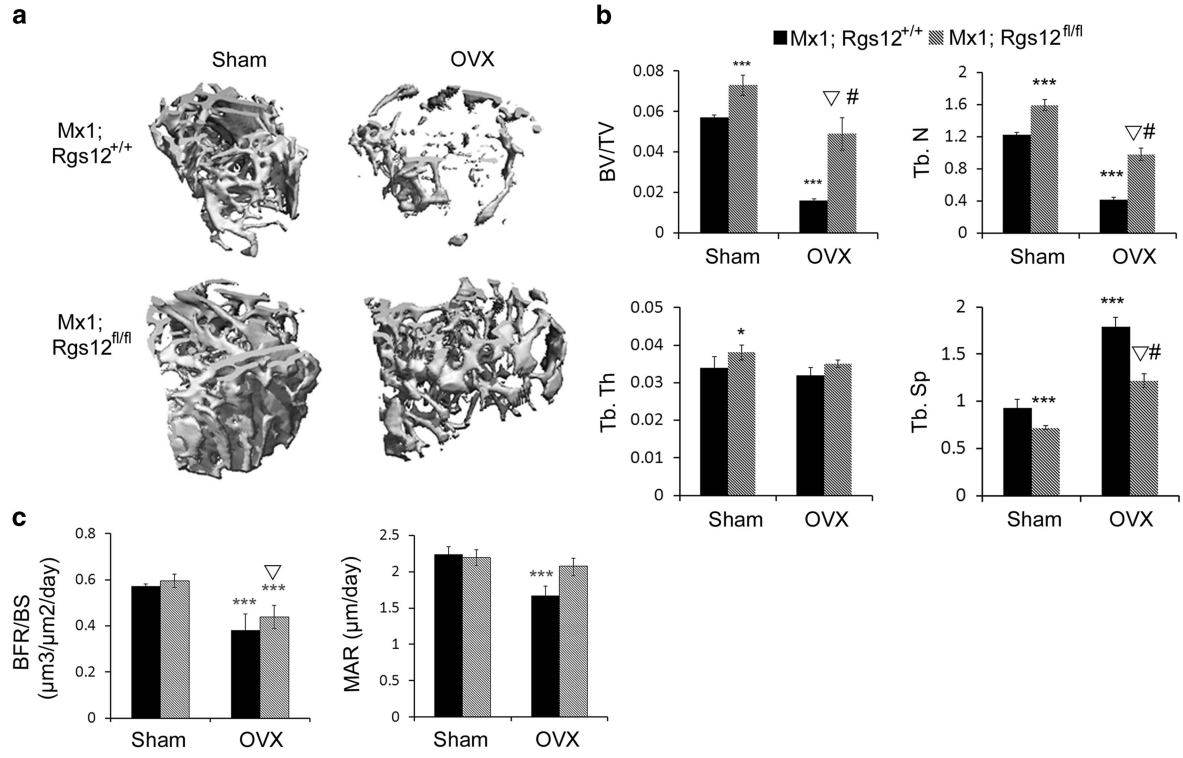

Figure 8 Mx1;Rgs12$^{fl/fl}$ were partially protected from OVX-induced bone loss. (**a**) Tibias from sham-operated and OVX mice were examined by μCT. (**b**) Quantitative analysis of bone volume/tissue volume (BV/TV, %), trabecular thickness (Tb.Th, μm), trabecular number (Tb.N, /mm), and trabecular separation (Tb.Sp, μm) in the tibia of Mx1; Rgs12$^{fl/fl}$ and Mx1;Rgs12$^{+/+}$ mice in the OVX and sham groups shown in panel (**a**) ($n=5$). (**c**) Quantification of BFR/BS (mm^3/mm^2/day) and the MAR (μd/day). Data represent mean $\pm$ S.D. $n=5$. $^*P<0.05$; $^{***}P<0.001$ compared with Mx1;Rgs12$^{+/+}$ sham. $^{\#}P<0.01$ Mx1;Rgs12$^{fl/fl}$ OVX *versus* Mx1;Rgs12$^{fl/fl}$ sham; $\triangledown P<0.01$ Mx1;Rgs12$^{fl/fl}$ OVX *versus* Mx1;Rgs12$^{+/+}$ OVX

CD11b;Rgs12$^{fl/fl}$ group than in the control group, demonstrating that Rgs12 likely regulates LPS-induced osteoclastogenesis through the regulation of NFAT2 expression and activation. Inhibition of Rgs12 might be a promising approach to treating inflammation-induced bone loss diseases.

Estrogen is a female hormone that helps to maintain healthy bones. Women after menopause are at a high risk for osteoporosis due to lower levels of estrogen.[48] The use of OVX animals is common to investigate postmenopausal osteoporosis and to facilitate the development of new treatments for this disease.[49] OVX mouse is a powerful tool for the study of pathogenesis of postmenopausal osteoporosis using various transgenic mice. In OVX-induced aging mice, we found that mice lacking Rgs12 in OC precursors were partially protected from age-associated bone loss. We detected much higher BV/TV, Tb.N, and trabecular spacing, as well as a slight increase in MAR and BFR/BS in Mx1;Rgs12$^{fl/fl}$ and Mx1; Rgs12$^{+/+}$ mice. This could be due to the involvement of Wolff's Law. Wolff's law-induced adaption should result in an increase of OBs and OCs. However, because of markedly inhibited OC differentiation in Mx1;Rgs12$^{fl/fl}$ mice, relatively increased OBs and decreased OCs cause unbalanced bone formation and resorption, which favors bone formation in Mx1;Rgs12$^{fl/fl}$. Most recently, it was reported that Mx1 is also expressed in a subset of mesenchymal stem cells (MSCs).[50] These Mx1$^+$ MSCs are OB lineage-restricted stem/progenitor cells that respond to tissue stress and migrate to sites of injury, supplying new OBs during fracture healing. Thus we cannot rule out the possibility that Rgs12 exerts a slight effect on OB function that results in a measurable change in BFR/BS and MAR. However, our data demonstrated that the OC dysfunction predominated, resulting in an overall increase in BV/TV.

In summary, we demonstrated that Rgs12 has a crucial role in the function of bone-resorbing OCs, particularly in preclinical models of pathological bone loss associated with inflammation-induced bone loss and postmenopausal osteoporosis. Our data suggest that Rgs12 has potential as a novel drug target for preventing postmenopausal osteoporosis and inflammation-induced bone loss.

Materials and Methods

Generation of Rgs12 conditional knockout mice. Methodology for generation of Rgs12$^{fl/fl}$, Mx1-Cre, and CD11b-Cre mice have been previously described.[22,23,25] To generate Rgs12$^{fl/+}$;CD11b-Cre mice, Rgs12$^{fl/fl}$ mice were crossed with CD11b-Cre transgenic mice. To generate Rgs12$^{fl/fl}$;CD11b-Cre mice (referred to as CD11b;Rgs12$^{fl/fl}$), female Rgs12$^{fl/fl}$ mice were crossed with male Rgs12$^{fl/+}$;CD11b-Cre mice. Because heterozygous Rgs12$^{fl/+}$;CD11b-Cre mice (CD11b;Rgs12$^{fl/+}$) were indistinguishable from wild-type mice, CD11b;Rgs12$^{fl/+}$ mice from the same litter of CD11b;Rgs12$^{fl/fl}$ mice were used as control.

Mx1;Rgs12$^{fl/fl}$ mice were generated by crossing Rgs12$^{fl/fl}$ mice with Mx1-Cre mice, which express Cre recombinase under the control of a type I interferon-inducible MX1 promoter. Activation of MX1-Cre was accomplished by intraperitoneal injection of poly I:C. Mx1;Rgs12$^{fl/fl}$ and Mx1;Rgs12$^{+/+}$ mice were injected with 0.25 ml of poly I:C (1 mg/ml) in phosphate-buffered saline (PBS) at postnatal days 10, 12, and 14.[24]

Genotyping of mice was performed by PCR of proteinase K-digested tail or spleen DNA as we have previously done.[25] The Cre transgene was detected using primer CreF (5′-CCTGGAAAATGCTT CTGTCCGTTTGCC-3′) and primer CreB (5′-GGCGCGGCAACACCATTTTT-3′). The deleted, floxed, and wild-type alleles

were genotyped using three primers: S (5′-CAGTTATTGGAAACTATCTCATGAC-3′); M (5′-TCCCCAAGCCTCTTACTTCA-3′); and W (5′-CACCGCACACACAAAATAAA TATCA-3′). All experimental mice (CD11b;Rgs12$^{fl/fl}$ and CD11b;Rgs12$^{fl/+}$) were male because transgene integration of CD11b-Cre is on the Y chromosome.[22]

All animal studies were approved by University at Buffalo Institutional Animal Care and Use Committee.

Isolation of CD11b-positive cells from bone marrow cells. CD11b-positive cells were isolated from the bone marrow cells from CD11b;Rgs12$^{+/+}$ and CD11b;Rgs12$^{fl/+}$ mice using a CD11b MicroBeads kit (Miltenyi Biotec Inc., Auburn, CA, USA) following the manufacturer's instructions. CD11b-positive cells were subjected to *Rgs12* expression analysis by using quantitative real-time PCR (qPCR) and western blotting.

qPCR. Total RNA was isolated from the spleen, cultured OCs or CD11b-positive cells from mouse bone marrow using Trizol reagent (Invitrogen, Carlsbad, CA, USA), following the manufacturer's instructions. cDNA was synthesized from 2 μg total RNA using the RNA to cDNA EcoDry Premix kit (Clontech, Palo Alto, CA, USA). Primers were designed with the IDT SCI primer design tool (Integrated DNA Technologies, San Diego, CA, USA). qPCR experiments were performed on an ABI PRISM 7500 real-time PCR system (Invitrogen) with SYBR Green PCR master Mix (Invitrogen). Sequences and product lengths for each primer pair were as follows: Rgs12 (Forward: 5′-GTGACCGTTGATGCTTTCG-3′; Reverse: 5′-ATCGCATG TCCCACTATTCC-3′, 132 bp); Cathepsin K (Forward: 5′-GCATTACCAACATGGC CAGC -3'; Reverse: 5′-CTCCCTTCCAAAGCCACCAA-3′; 109 bp); c-Fos (Forward: 5′-CGACCATGATGTTCTCGGGT-3′; Reverse: 5′-TCGGCTGGGGAATGGTAGTA -3′; 109 bp); NFAT2 (Forward: 5′-ATATGAGCCCATCCTTGCCTGCC-3′; Reverse: 5′-TTGGGCTGCACCTCGATCCG-3′, 85 bp); and GAPDH (Forward: 5′-TGTGTC CGTCGTGGATCTGA-3′; Reverse 5′-TTGCTGTTGAAGTCGCAGGAG-3′; 150 bp). All reactions were run in triplicate and normalized to the housekeeping gene GAPDH.

Western blotting. Western blotting was used to detect RGS12 using the chicken anti-Rgs12 antibody (1 : 500, Abcam, Cambridge, MA, USA). For Mx1; Rgs12$^{fl/fl}$ mice, bone marrow from poly I:C-induced mice were harvested. For CD11b;Rgs12$^{fl/fl}$ mice, bone marrow cells were purified with CD11b MicroBeads Kit. All samples were homogenized with RIPA buffer (50 mM Tris, 150 mM NaCl, 1% Triton X-100, 0.1% SDS and 1% sodium deoxycholate) combined with protease inhibitor cocktail (Sigma, St Louis, MO, USA). About 20–40 μg proteins were loaded and separated in 10% SDS-PAGE gels and transferred to polyvinylidene difluoride membranes. The membranes were incubated with primary antibody overnight at 4 °C and then incubated with horseradish peroxidase–conjugated secondary antibodies at room temperature for 1 h. Visualization was done with WesternBright ECL HRP (Advansta, Menlo Park, CA, USA). GAPDH (1 : 2000, Genscript, Piscataway, NJ, USA) was used as the internal control.

Radiographic procedures and quantitative Micro-CT measurements. Radiography was performed by using Siemens X-ray equipment (Siemens, Madison, WI, USA) with high-speed holographic film (Kodak, Rochester, NY, USA). A quantitative analysis of the gross bone morphology and microarchitecture was performed by a Micro-CT system (USDA Grand Forks Human Nutrition Research Center, Grand Forks, ND, USA). Fixed femur from Rgs12 mutant and Cre control mice ($n=4$) were analyzed and 3D reconstitution was used to determine bone volume (BV/TV), trabecular number (Tb.N), and trabecular thickness (Tb.Th) as described.[25,51,52]

Histology and histomorphometric analyses. Mice femurs and tibias were excised, fixed for 24 h in 10% natural buffered formalin, and decalcified in 10% EDTA for 1–2 weeks at 4 °C. The samples were embedded in paraffin and then sectioned at 5 μm and stained with H&E ($n=4$).

TRAP staining was performed after deparaffinization using an acid phosphatase, leukocyte (TRAP) Kit (Sigma). OC number per bone surface (N.Oc/B.S, *n*/mm^2) and the percentage of OC surface to bone surface (Oc.S/B.S, %) were calculated by counting TRAP$^+$ cells and measuring the area in sagittal histological sections of the tibia (normalized to the total bone surface) using the Image J software (US National Institutes of Health, Bethesda, MA, USA) ($n=4$).

***In vitro* osteoclastogenesis and retroviral gene transfer.** Non-adherent bone marrow cells were obtained from the tibia and femur bone marrow cavity of CD11b;Rgs12$^{fl/fl}$ and CD11b;Rgs12$^{+/+}$ mice as described.[21] Briefly, bone marrow was flushed from long bones, dispersed into single cells, and cultured with α-Minimal Essential Medium (α-MEM, Gibco BRL Invitrogen, Carlsbad, CA, USA) containing 10% fetal bovine serum (FBS) (Atlanta Biologicals, Lawrenceville, GA, USA) and 20 ng/ml recombinant mouse macrophage colony-stimulating factor (M-CSF) (R&D Systems, Minneapolis, MN, USA) for 24 h and then used as OC precursor cells. Nonadherent cells were harvested and continuously cultured in the presence of 10 ng/ml RANKL (ProSpec-Tany TechnoGene Ltd., Ness Ziona, Israel) and 20 ng/ml M-CSF for 4–5 days to generate mature OCs.

The co-culture model was set up as previously described.[53] Bone marrow cells (1x10^6 cells/well) were cultured with wild-type primary OBs (calvarial bone derived) (1x10^5 cells/well) in α-MEM containing 10% FBS, 10^{-7} M dexamethasone and 10^{-8} M 1α, 25-dihydroxyvitamin D_3 (Sigma, D1530) in 24-well plates for 6–7 days.[26,54]

For rescue experiments, ca-NFAT2 retrovirus was generated with ca-NFAT2 vector (Addgene plasmid 11102, Cambridge, MA, USA) and phoenix Eco packaging cells (Garry Nolan, Stanford University, Stanford, CA, USA) as previously described.[55] Nonadherent bone marrow cells were cultured with M-CSF for another 24 h and incubated with viral supernatant for 8 h in the presence of 8 μg/ml polybrene.[40,56,57] After removing the viral-containing medium, the cells were cultured with 20 ng/ml M-CSF and 10 ng/ml RANKL for 3–4 days. OCs were stained with TRAP and analyzed by using qPCR.

TRAP staining was performed at the end with the acid phosphatase, using leukocyte (TRAP) Kit (Sigma). The osteoclastogenesis level was determined by counting the number of TRAP$^+$ multinucleated cells (MNCs, >3 nuclei/cell) per well under $\times 20$ magnification. The experiments were carried out in quadruplicate.

Fluorescent staining for actin ring of OCs. OCs generated from RANKL induction or co-culture were fixed with 3.7% formaldehyde solution in PBS for 10 min at room temperature and permeabilized with ice-cold acetone at -20 °C for 5 min. OC actin rings were stained with rhodamine–phalloidin (Sigma, R415) (1 : 40 dilution) following the manufacturer's instructions. After staining, 4,6-diamidino-2-phenylindole (DAPI) (Sigma) was added and used as a counterstain for nuclei. Actin rings were analyzed by using Zeiss Axio imager microscope (Carl Zeiss, Jena, Germany). The calculation of the normal actin rings and disrupted actin rings were performed as described.[29,58] Briefly, an actin ring with less than half a ring was counted as the disrupted ring, and OCs were identified by the presence of more than two nuclei. The experiments were repeated independently three times.

Dentin resorption assay. Dentin resorption assay was performed as previously described with minor modifications.[21,59] Briefly, bone marrow cells were plated on the transverse slices of elephant dentin (Elephant Ivory Tusks, FL, USA) in 24-well plate and induced with α-MEM containing 10% FBS (pH 6.9), 20 ng/ml M-CSF, and 10 ng/ml RANKL. After 6 days in culture, OCs were removed by sonication, and the resorbed area was measured using Hitachi SU70 scanning electron microscope (Hitachi Instruments, Schaumburg, IL, USA) ($n=3$).

Ca^{2+} oscillation measurement. Ca^{2+} oscillation measurements were performed as previously described with minor modification.[13,21] Nonadherent bone marrow cells from CD11b;Rgs12$^{fl/+}$ and CD11b;Rgs12$^{fl/fl}$ mice were induced with 20 ng/ml M-CSF and 10 ng/ml RANKL for 24 h. The cells were loaded with 5 μM fluo-4 AM (Invitrogen) for 30 min in α-MEM containing 0.05% pluronic F127 (Sigma) and washed in Hank's Balanced Salt Solution. Intracellular Ca^{2+} concentration change was accessed by using a Zeiss Axio imager Motorized fluorescence microscope. The cells were excited at 488 nm, and the emission signals for 505–530 nm were recorded simultaneously at 5-s intervals for 5 min. The fluorescence intensity was calculated using the Image J software and plotted over time ($n=5$).

LPS-induced osteogenesis and bone erosion. CD11b;Rgs12$^{fl/+}$ and CD11b;Rgs12$^{fl/fl}$ mice (7–8 weeks old, $n=8$) were administered a local calvarial injection of LPS (Sigma, 02:B6, L8274) or PBS (sham group) at 25 mg per kg body weight.[34–37] A 27.5-gauge needle was used, and the injection site was at the point on the midline of the skull located between the ears and eyes. Five days after the initial injection, the mice were euthanized, and histological sections of the calvarial bones were prepared as described above. The levels of osteogenesis and bone loss were assessed by H&E and TRAP staining. Bone resorption was calculated by measuring the ratio of eroded surface over total bone surface. The OC number per bone surface[29] was calculated as described above.

LPS-induced *in vitro* osteoclastogenesis was performed as previously reported.[47] Bone marrow cells from CD11b;Rgs12$^{fl/+}$ and CD11b;Rgs12$^{fl/fl}$ mice were cultured

with α-MEM containing 10% FBS, 20 ng/ml M-CSF, and 10 ng/ml RANKL for 36 h and then cultured with α-MEM containing 10% FBS, 20 ng/ml M-CSF, and 100 ng/ml LPS for 5 days. TRAP staining was performed to evaluate OC formation ($n=3$).

Ovariectomy. Either ovariectomy or a sham operation was performed in 4-month-old Mx1;Rgs12$^{+/+}$ and Mx1;Rgs12$^{fl/fl}$ females ($n=5$ for each group) as reported previously.[60,61] Three-month-old mice were anesthetized with 1000 cc/min O_2 and 5% isofluorane. Ovaries were approached by two separate flank incisions. The ovary and the oviduct were exteriorized and removed with single cut. The ligated uterine horn was replaced into the peritoneal cavity. The muscle and skin were sutured. In the sham group, ovaries were only touched with forceps. The mice were killed 6 weeks after OVX. One femur was excised for Micro-CT examination.

Statistical analysis. All data are expressed as mean $\pm$ S.D. ($n=\geq 3$). Student's *t*-test for the comparison between two groups or one-way ANOVA followed by Tukey's multiple-comparison posttest for multiple groups was performed. $P<0.05$ was considered to be significant.

Conflict of Interest

The authors declare no conflict of interest.

Acknowledgements. We thank Dr Kristina Wasson-Blader and Miss Stacy Scheuneman for editing the manuscript, Dr Wade J Sigurdson, the director of the Flow Cytometry Facility at the School of Medicine and Biomedical Sciences, University at Buffalo, for assistance with the fluorescence microscope and Dr Peter J Bush for the technical assistance in using scanning electron microscope. This work was supported by the National Institute of Arthritis and Musculoskeletal and Skin Diseases and National Institute of Aging under Award Numbers AR061052, AR066101 and AG048388 (to SY) and the USDA Agricultural Research Service program 'Bone Metabolism in Obesity,' Current Research Information System no. 5450-51000-046-00D to JC.

1. Zaidi M. Skeletal remodeling in health and disease. *Nat Med* 2007; **13**: 791–801.
2. Kawai M, Modder UI, Khosla S, Rosen CJ. Emerging therapeutic opportunities for skeletal restoration. *Nat Rev Drug Discov* 2011; **10**: 141–156.
3. Lories R. The balance of tissue repair and remodeling in chronic arthritis. *Nat Rev Rheumatol* 2011; **7**: 700–707.
4. Weitzmann MN. The role of inflammatory cytokines, the RANKL/OPG axis, and the immunoskeletal interface in physiological bone turnover and osteoporosis. *Scientifica (Cairo)* 2013; **2013**: 125705.
5. Boyce BF. Advances in osteoclast biology reveal potential new drug targets and new roles for osteoclasts. *J Bone Miner Res* 2013; **28**: 711–722.
6. Boyce BF, Rosenberg E, de Papp AE, Duong le T. The osteoclast, bone remodelling and treatment of metabolic bone disease. *Eur J Clin Invest* 2012; **42**: 1332–1341.
7. Boyle WJ, Simonet WS, Lacey DL. Osteoclast differentiation and activation. *Nature* 2003; **423**: 337–342.
8. Nakagawa N, Kinosaki M, Yamaguchi K, Shima N, Yasuda H, Yano K *et al.* RANK is the essential signaling receptor for osteoclast differentiation factor in osteoclastogenesis. *Biochem Biophys Res Commun* 1998; **253**: 395–400.
9. Hsu H, Lacey DL, Dunstan CR, Solovyev I, Colombero A, Timms E *et al.* Tumor necrosis factor receptor family member RANK mediates osteoclast differentiation and activation induced by osteoprotegerin ligand. *Proc Natl Acad Sci USA* 1999; **96**: 3540–3545.
10. Martin TJ. Historically significant events in the discovery of RANK/RANKL/OPG. *World J Orthop* 2013; **4**: 186–197.
11. Asagiri M, Takayanagi H. The molecular understanding of osteoclast differentiation. *Bone* 2007; **40**: 251–264.
12. Song I, Kim JH, Kim K, Jin HM, Youn BU, Kim N. Regulatory mechanism of NFATc1 in RANKL-induced osteoclast activation. *FEBS Lett* 2009; **583**: 2435–2440.
13. Takayanagi H, Kim S, Koga T, Nishina H, Isshiki M, Yoshida H *et al.* Induction and activation of the transcription factor NFATc1 (NFAT2) integrate RANKL signaling in terminal differentiation of osteoclasts. *Dev Cell* 2002; **3**: 889–901.
14. Negishi-Koga T, Takayanagi H. Mysteries in Ca2+ signaling during osteoclast differentiation. *IBMS Bonekey* 2009; **6**: 301–306.
15. Snow BE, Antonio L, Suggs S, Gutstein HB, Siderovski DP. Molecular cloning and expression analysis of rat Rgs12 and Rgs14. *Biochem Biophys Res Commun* 1997; **233**: 770–777.
16. Schiff ML, Siderovski DP, Jordan JD, Brothers G, Snow B, De Vries L *et al.* Tyrosine-kinase-dependent recruitment of RGS12 to the N-type calcium channel. *Nature* 2000; **408**: 723–727.
17. Snow BE, Brothers GM, Siderovski DP. Molecular cloning of regulators of G-protein signaling family members and characterization of binding specificity of RGS12 PDZ domain. *Methods Enzymol* 2002; **344**: 740–761.
18. Sambi BS, Hains MD, Waters CM, Connell MC, Willard FS, Kimple AJ *et al.* The effect of RGS12 on PDGFbeta receptor signalling to p42/p44 mitogen activated protein kinase in mammalian cells. *Cell Signal* 2006; **18**: 971–981.
19. Snow BE, Hall RA, Krumins AM, Brothers GM, Bouchard D, Brothers CA *et al.* GTPase activating specificity of RGS12 and binding specificity of an alternatively spliced PDZ (PSD-95/Dlg/ZO-1) domain. *J Biol Chem* 1998; **273**: 17749–17755.
20. Willard MD, Willard FS, Li X, Cappell SD, Snider WD, Siderovski DP. Selective role for RGS12 as a Ras/Raf/MEK scaffold in nerve growth factor-mediated differentiation. *EMBO J* 2007; **26**: 2029–2040.
21. Yang S, Li YP. RGS12 is essential for RANKL-evoked signaling for terminal differentiation of osteoclasts in vitro. *J Bone Miner Res* 2007; **22**: 45–54.
22. Ferron M, Vacher J. Targeted expression of Cre recombinase in macrophages and osteoclasts in transgenic mice. *Genesis* 2005; **41**: 138–145.
23. Kuhn R, Schwenk F, Aguet M, Rajewsky K. Inducible gene targeting in mice. *Science* 1995; **269**: 1427–1429.
24. Aliprantis AO, Ueki Y, Sulyanto R, Park A, Sigrist KS, Sharma SM *et al.* NFATc1 in mice represses osteoprotegerin during osteoclastogenesis and dissociates systemic osteopenia from inflammation in cherubism. *J Clin Invest* 2008; **118**: 3775.
25. Yang S, Li YP, Liu T, He X, Yuan X, Li C *et al.* Mx1-Cre mediated Rgs12 conditional knockout mice exhibit increased bone mass phenotype. *Genesis* 2013; **51**: 201–209.
26. Suda T, Jimi E, Nakamura I, Takahashi N. Role of 1 alpha,25-dihydroxyvitamin D3 in osteoclast differentiation and function. *Methods Enzymol* 1997; **282**: 223–235.
27. Bradley EW, Oursler MJ. Osteoclast culture and resorption assays. *Osteoporosis*. Springer: New York City, 2008, pp 19–35.
28. Marchisio PC, Cirillo D, Naldini L, Primavera MV, Teti A, Zambonin-Zallone A. Cell-substratum interaction of cultured avian osteoclasts is mediated by specific adhesion structures. *J Cell Biol* 1984; **99**: 1696–1705.
29. Wilson SR, Peters C, Saftig P, Bromme D. Cathepsin K activity-dependent regulation of osteoclast actin ring formation and bone resorption. *J Biol Chem* 2009; **284**: 2584–2592.
30. Zeng W, Xu X, Popov S, Mukhopadhyay S, Chidiac P, Swistok J *et al.* The N-terminal domain of RGS4 confers receptor-selective inhibition of G protein signaling. *J Biol Chem* 1998; **273**: 34687–34690.
31. Taylor CW, Thorn P. Calcium signalling: IP3 rises again...and again. *Curr Biol* 2001; **11**: R352–R355.
32. Ishii M, Kurachi Y. Physiological actions of regulators of G-protein signaling (RGS) proteins. *Life Sci* 2003; **74**: 163–171.
33. Ishii M, Fujita S, Yamada M, Hosaka Y, Kurachi Y. Phosphatidylinositol 3,4,5-trisphosphate and Ca2+/calmodulin competitively bind to the regulators of G-protein-signalling (RGS) domain of RGS4 and reciprocally regulate its action. *Biochem J* 2005; **385**: 65–73.
34. Li L, Khansari A, Shapira L, Graves DT, Amar S. Contribution of interleukin-11 and prostaglandin(s) in lipopolysaccharide-induced bone resorption in vivo. *Infect Immun* 2002; **70**: 3915–3922.
35. Ohishi M, Matsumura Y, Aki D, Mashima R, Taniguchi K, Kobayashi T *et al.* Suppressors of cytokine signaling-1 and -3 regulate osteoclastogenesis in the presence of inflammatory cytokines. *J Immunol* 2005; **174**: 3024–3031.
36. Takayanagi H, Kim S, Matsuo K, Suzuki H, Suzuki T, Sato K *et al.* RANKL maintains bone homeostasis through c-Fos-dependent induction of interferon-beta. *Nature* 2002; **416**: 744–749.
37. Takayanagi H, Ogasawara K, Hida S, Chiba T, Murata S, Sato K *et al.* T-cell-mediated regulation of osteoclastogenesis by signalling cross-talk between RANKL and IFN-gamma. *Nature* 2000; **408**: 600–605.
38. Beamer WG, Shultz KL, Donahue LR, Churchill GA, Sen S, Wergedal JR *et al.* Quantitative trait loci for femoral and lumbar vertebral bone mineral density in C57BL/6 J and C3H/HeJ inbred strains of mice. *J Bone Miner Res* 2001; **16**: 1195–1206.
39. Miles RR, Sluka JP, Santerre RF, Hale LV, Bloem L, Boguslawski G *et al.* Dynamic regulation of RGS2 in bone: potential new insights into parathyroid hormone signaling mechanisms. *Endocrinology* 2000; **141**: 28–36.
40. Yang S, Li YP. RGS10-null mutation impairs osteoclast differentiation resulting from the loss of [Ca2+]i oscillation regulation. *Genes Dev* 2007; **21**: 1803–1816.
41. Zumsteg A, Baeriswyl V, Imaizumi N, Schwendener R, Ruegg C, Christofori G. Myeloid cells contribute to tumor lymphangiogenesis. *PLoS One* 2009; **4**: e7067.
42. Hollinger S, Hepler JR. Cellular regulation of RGS proteins: modulators and integrators of G protein signaling. *Pharmacol Rev* 2002; **54**: 527–559.
43. Aeschlimann D, Evans B. The vital osteoclast: how is it regulated? *Cell Death Differ* 2004; **11**: S5–S7.
44. Chiang CY, Kyritsis G, Graves DT, Amar S. Interleukin-1 and tumor necrosis factor activities partially account for calvarial bone resorption induced by local injection of lipopolysaccharide. *Infect Immun* 1999; **67**: 4231–4236.
45. Hirschfeld M, Ma Y, Weis JH, Vogel SN, Weis JJ. Cutting edge: repurification of lipopolysaccharide eliminates signaling through both human and murine toll-like receptor 2. *J Immunol* 2000; **165**: 618–622.
46. Nair SP, Meghji S, Wilson M, Reddi K, White P, Henderson B. Bacterially induced bone destruction: mechanisms and misconceptions. *Infect Immun* 1996; **64**: 2371–2380.

47. Liu J, Wang S, Zhang P, Said-Al-Naief N, Michalek SM, Feng X. Molecular mechanism of the bifunctional role of lipopolysaccharide in osteoclastogenesis. *J Biol Chem* 2009; **284**: 12512–12523.
48. Society NAM. Management of osteoporosis in postmenopausal women: 2006 position statement of the North American Menopause Society. *Menopause (New York)* 2006; **13**: 340.
49. Kalu DN. The ovariectomized rat model of postmenopausal bone loss. *Bone Miner* 1991; **15**: 175–191.
50. Park D, Spencer JA, Koh BI, Kobayashi T, Fujisaki J, Clemens TL *et al.* Endogenous bone marrow MSCs are dynamic, fate-restricted participants in bone maintenance and regeneration. *Cell Stem Cell* 2012; **10**: 259–272.
51. Bensamoun SF, Hawse JR, Subramaniam M, Ilharreborde B, Bassillais A, Benhamou CL *et al.* TGFbeta inducible early gene-1 knockout mice display defects in bone strength and microarchitecture. *Bone* 2006; **39**: 1244–1251.
52. Hawse JR, Iwaniec UT, Bensamoun SF, Monroe DG, Peters KD, Ilharreborde B *et al.* TIEG-null mice display an osteopenic gender-specific phenotype. *Bone* 2008; **42**: 1025–1031.
53. Wang Y, Liu W, Masuyama R, Fukuyama R, Ito M, Zhang Q *et al.* Pyruvate dehydrogenase kinase 4 induces bone loss at unloading by promoting osteoclastogenesis. *Bone* 2012; **50**: 409–419.
54. Arai F, Miyamoto T, Ohneda O, Inada T, Sudo T, Brasel K *et al.* Commitment and differentiation of osteoclast precursor cells by the sequential expression of c-Fms and receptor activator of nuclear factor kappaB (RANK) receptors. *J Exp Med* 1999; **190**: 1741–1754.
55. Monticelli S, Rao A. NFAT1 and NFAT2 are positive regulators of IL-4 gene transcription. *Eur J Immunol* 2002; **32**: 2971–2978.
56. Kim K, Kim JH, Lee J, Jin HM, Lee SH, Fisher DE *et al.* Nuclear factor of activated T cells c1 induces osteoclast-associated receptor gene expression during tumor necrosis factor-related activation-induced cytokine-mediated osteoclastogenesis. *J Biol Chem* 2005; **280**: 35209–35216.
57. Kim K, Lee SH, Ha Kim J, Choi Y, Kim N. NFATc1 induces osteoclast fusion via up-regulation of Atp6v0d2 and the dendritic cell-specific transmembrane protein (DC-STAMP). *Mol Endocrinol* 2008; **22**: 176–185.
58. Lakkakorpi PT, Horton MA, Helfrich MH, Karhukorpi EK, Vaananen HK. Vitronectin receptor has a role in bone resorption but does not mediate tight sealing zone attachment of osteoclasts to the bone surface. *J Cell Biol* 1991; **115**: 1179–1186.
59. Tamura T, Takahashi N, Akatsu T, Sasaki T, Udagawa N, Tanaka S *et al.* New resorption assay with mouse osteoclast-like multinucleated cells formed in vitro. *J Bone Miner Res* 1993; **8**: 953–960.
60. Lai CF, Cheng SL, Mbalaviele G, Donsante C, Watkins M, Radice GL *et al.* Accentuated ovariectomy-induced bone loss and altered osteogenesis in heterozygous N-cadherin null mice. *J Bone Miner Res* 2006; **21**: 1897–1906.
61. Su X, Floyd DH, Hughes A, Xiang J, Schneider JG, Uluckan O *et al.* The ADP receptor P2RY12 regulates osteoclast function and pathologic bone remodeling. *J Clin Invest* 2012; **122**: 3579.

Supplementary Information accompanies this paper on Cell Death and Differentiation website (http://www.nature.com/cdd)